# InGaAsP/InP quantum-well electrorefractive modulators with sub-volt $V_\pi$

Paul W. Juodawlkis[a], Frederick J. O'Donnell[a], Robert J. Bailey[a], Jason J. Plant[a], Kevin G. Ray[a], Douglas C. Oakley[a], Antonio Napoleone[a], Michael R. Watts[b], and Gary E. Betts[c]

[a]Lincoln Laboratory, Massachusetts Institute of Technology, Lexington, MA 02420
[b]Department of Electrical Engineering and Computer Science, Massachusetts Institute of Technology, Cambridge, MA 02142
[c]Ipitek, Carlsbad, CA 92008

## ABSTRACT

Advanced analog-optical sensor, signal processing and communication systems could benefit significantly from wideband (DC to > 50 GHz) optical modulators having both low half-wave voltage ($V_\pi$) and low optical insertion loss. An important figure-of-merit for modulators used in analog applications is $T_{MAX}/V_\pi$, where $T_{MAX}$ is the optical transmission of the modulator when biased for maximum transmission. Candidate electro-optic materials for realizing these modulators include lithium niobate ($LiNbO_3$), polymers, and semiconductors, each of which has its own set of advantages and disadvantages. In this paper, we report the development of 1.5-μm-wavelength Mach-Zehnder modulators utilizing the electrorefractive effect in InGaAsP/InP symmetric, uncoupled semiconductor quantum-wells. Modulators with 1-cm-long, lumped-element electrodes are found to have a push-pull $V_\pi$ of 0.9V ($V_\pi L$ = 9 V-mm) and 18-dB fiber-to-fiber insertion loss ($T_{MAX}/V_\pi$ = 0.018). Fabry-Perot cutback measurements reveal a waveguide propagation loss of 7 dB/cm and a waveguide-to-fiber coupling loss of 5 dB/facet. The relatively high propagation loss results from a combination of below-bandedge absorption and scattering due to waveguide-sidewall roughness. Analyses show that most of the coupling loss can be eliminated though the use of monolithically integrated inverted-taper optical-mode converters, thereby allowing these modulators to exceed the performance of commercial $LiNbO_3$ modulators ($T_{MAX}/V_\pi \sim 0.1$). We also report the analog modulation characteristics of these modulators.

**Keywords:** optical modulator, analog, quantum well, semiconductor, Mach-Zehnder, electrorefraction

## 1. INTRODUCTION

Wideband, low-loss, high-dynamic-range analog optical links are an enabling technology for applications such as antenna remoting,[1] signal distribution and manipulation on phased-array antennas,[2] and transmission of millimeter-wave radio-over-fiber signals.[3] For applications demanding dynamic range exceeding ~110 dB, external modulation is typically required.[4] In an externally modulated analog link, the transmitter consists of a continuous-wave (CW) laser and an optical modulator that impresses the analog signal onto the optical carrier. An important performance metric for an analog link is the radio-frequency (RF) gain, which is defined as the ratio of the RF power delivered to the output load ($P_L$) and the RF power from the input source ($P_S$). For an intensity-modulated link using external modulation, the RF gain can be expressed as[5]

$$G_{RF} = \frac{P_L}{P_S} = \left( \frac{P_{O,M}^2}{P_S} \right) \cdot T_F^2 \cdot \left( \frac{P_L}{P_{O,D}^2} \right) = \left( \frac{s_M^2}{R_M} \right) \cdot T_F^2 \cdot \left( s_D^2 R_L \right) \quad (1)$$

where $P_{O,M}$ is the optical power at the output of the modulator, $T_F$ is the fractional transmission between the modulator output and the photodetector input, $P_{O,D}$ is the power at the input to the photodetector, $s_M$ is the modulator slope efficiency (W/A), $R_M$ is the modulator impedance, $s_D$ is the photodetector efficiency (A/W) and $R_L$ is the load impedance. For a Mach-Zehnder (MZ) interferometric modulator, the slope efficiency can be written as



Enabling Photonic Technologies for Aerospace Applications VI, edited by Andrew R. Pirich, Michael J. Hayduk, Eric Donkor, Proceedings of SPIE Vol. 5435 (SPIE, Bellingham, WA, 2004) · 0277-786X/04/$15 · doi: 10.1117/12.546786

$$s_M = \frac{dP_{O,M}}{dI_M} = \frac{\pi R_M P_O}{2} \cdot \left( \frac{T_{MAX}}{V_\pi} \right) \tag{2}$$

where $I_M$ is the modulator drive current, $P_O$ is the optical power at the input to the modulator, $T_{MAX}$ is the maximum optical transmission of the modulator when it is biased fully ON, and $V_\pi$ is the modulator's half-wave voltage.

From Eqs. (1) and (2) it is evident that the relative modulator slope efficiency, $T_{MAX}/V_\pi$, is an important figure-of-merit for analog modulators. The RF link gain, which is proportional to $(T_{MAX}/V_\pi)^2$, can be increased by reducing the modulator's insertion loss, thereby increasing $T_{MAX}$, or by reducing $V_\pi$. Commercial 40-Gb/s $LiNbO_3$ modulators currently exhibit $T_{MAX}/V_\pi \sim 0.1$ $V^{-1}$ ($V_\pi$ = 5 V, Loss = 3 dB).[6] Semiconductor electroabsorption modulators with high-efficiency coupling have demonstrated $T_{MAX}/V_\pi \sim 0.15$ (effective $V_\pi$ = 2.2 V, Loss = 5 dB).[7]

Optical modulators having values of $T_{MAX}/V_\pi$ significantly greater than 0.1 $V^{-1}$ would greatly benefit both microwave analog-optical links and next-generation (> 10 Gb/s) digital-optical communication systems. Methods of reducing $V_\pi$ include increasing the effective electrical/optical interaction length via longer electrodes[8] or resonant enhancement,[9] or by using a material having a larger electro-optic coefficient. Semiconductor materials offer significantly stronger electro-optic effects than $LiNbO_3$ at fiber compatible wavelengths (1-1.7 μm) due to the ability to tailor the bandedge wavelength, allowing operation at wavelengths just below the bandedge. Both the electroabsorptive and electrorefractive effects in semiconductors have been used to implement optical modulators with low $V_\pi$.[10-15]

Figure 1 illustrates the effects of applying a voltage across a symmetric semiconductor quantum-well where the applied field is perpendicular to the plane of the well. When no voltage is applied (V = 0), the absorption spectrum near the bandedge consists of several sharp absorption-steps and resonances associated with the two-dimensional confinement of the quantum well.[16] In unstrained material, the bandedge is defined by the optical transition between the lowest heavy-hole (hh1) and electron (e1) energy levels. Under a zero-field condition, the overlap between the hh1 and e1 wavefunction envelopes is a maximum. When a voltage is applied (V > 0), the confinement potential of the well is altered as depicted in Fig. 1. This change in potential has two principal effects: (i) the confined energy levels of the electron and hole states decrease, causing the absorption bandedge to shift to longer wavelengths (red shift), and (ii) the

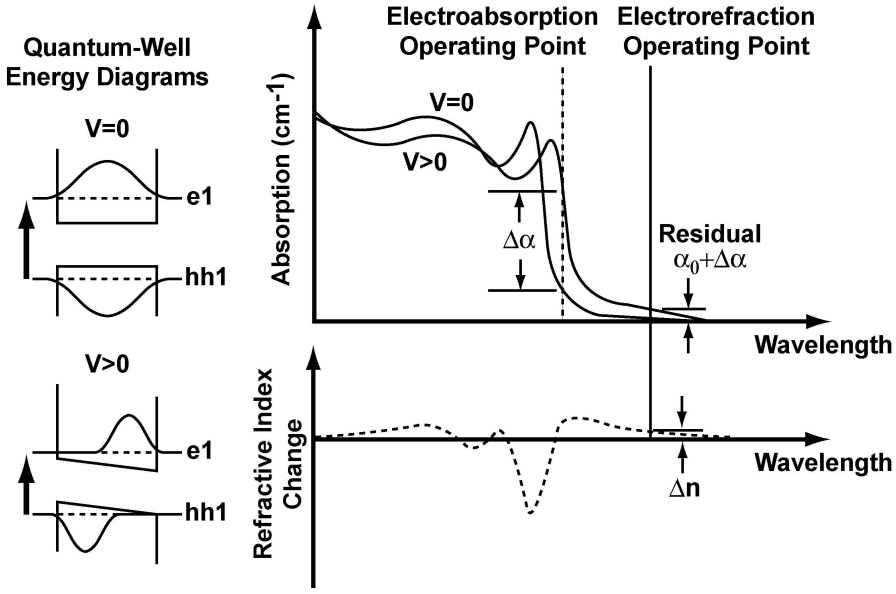


**Fig. 1**. Illustration of electroabsorptive and electrorefractive spectra in semiconductor quantum-well materials. Quantum-well energy band diagrams with and without and applied electric field are also shown. e1 = lowest-energy electron level. hh1 = lowest-energy heavy-hole level.

overlap of the symmetric electron and hole wavefunctions decrease, causing the magnitude of the bandedge absorption to decrease.[17] Both the bandedge red-shift and the absorption decrease are shown in Fig. 1. These changes in the quantum-well absorption with applied electric field are often referred to jointly as the quantum-confined Stark effect (QCSE).

Electroabsorption (EA) modulators use the voltage-dependent absorption changes directly. In a typical EA modulator, the quantum-well material is designed to position the bandedge at a wavelength slightly smaller (10-30 nm) than the wavelength of the incident optical signal when no voltage is applied to the modulator. When a voltage is applied, the bandedge red shifts and the optical signal is attenuated (see Fig. 1). A modulation efficiency vs. insertion loss trade-off exists since both the absorption change ($\Delta\alpha$) per applied volt and the residual absorption ($\alpha_0$) increase as the optical wavelength approaches the bandedge wavelength. An effective $V_\pi$ can be defined for EA modulators to allow comparison with interferometric modulators.[18] The linearity of an EA modulator is strongly dependent on the relative optical wavelength and the DC bias point of the modulator.[19]

In addition to changes in absorption, the QCSE also modifies the refractive index spectrum of the quantum well material.[20] The changes in refraction $\Delta n$ and absorption $\Delta\alpha$ are related through the Kramers-Kronig expressions. QCSE electrorefraction (ER) provides a larger electro-optic effect than $LiNbO_3$ because ER modulators are usually operated at wavelengths relatively near (100-150 nm) the bandedge resonance. However, whereas the electro-optic effect in $LiNbO_3$ has an extremely linear phase vs. applied voltage response, the ER phase-vs-voltage response is nonlinear. The exact ER phase-vs-voltage response is complicated, but it can be approximated as quadratic.[21] Additionally, the intrinsic material absorption of $LiNbO_3$ is very small ($< 0.01$ cm$^{-1}$) and relatively wavelength independent at 1.5-μm, whereas the below-bandedge absorption of quantum-well materials can be orders of magnitude larger and depends strongly on the difference between the bandedge and operating wavelengths. Thus, the increased electro-optic strength of an ER-based modulator can be offset by the below-bandedge absorption, thereby reducing $T_{MAX}/V_\pi$.

It is important to recognize that the bandedge red-shift and the bandedge-absorption reduction associated with the QCSE have competing effects on the below-bandedge refractive-index change $\Delta n$.[22] The bandedge shift results in a positive $\Delta n$ and the absorption reduction causes $\Delta n$ to be negative at wavelengths below the bandedge. Thus, these two components of the QCSE partially cancel the resulting $\Delta n$. Advanced quantum-well materials have been developed to enhance the electrorefractive strength by emphasizing one of the two QCSE-related changes. Stepped quantum wells exhibit a bandedge shift with little overlap-related absorption change.[23] Alternatively, asymmetric coupled quantum wells demonstrate a bandedge-absorption change with minimal bandedge shift.[22, 24]

In this paper, we report the demonstration of InGaAsP/InP ER Mach-Zehnder modulators incorporating uncoupled, symmetric quantum wells. We demonstrate modulators with 1-cm-long lumped-element modulators having push-pull $V_\pi = 0.9$ V and a fiber-to-fiber insertion loss of 18 dB. Cutback loss measurements reveal that 10 dB of this loss is due to fiber coupling. Analyses show that the total coupling loss could be reduced to less than 2 dB through the use of integrated optical mode-converters and anti-reflection coatings. We investigate the dependence of $T_{MAX}/V_\pi$ on the difference between the bandedge wavelength and the input optical wavelength. We also report the frequency response of the lumped-element electrode modulators and characterize the modulator linearity using two-tone intermodulation measurements.

## 2. ELECTROREFRACTIVE MODULATOR DESCRIPTION

The InGaAsP/InP ER modulator structures used in this investigation (Fig. 2) were grown via metal-organic chemical vapor deposition (MOCVD) on Fe-doped semi-insulating (100) InP substrates. The structures were n-i-p (i.e., p-doped layers nearest the substrate) rather than the typical p-i-n to minimize the series resistance. The inverted structure positions the low-resistivity n-type material in the narrow ridge region and increases the area of the high-resistivity p-type contact. The active region consists of 30 pairs of 12-nm InGaAsP wells and 8-nm InP barriers. The doping concentration near the waveguide core is low, especially on the p-side, to minimize the optical loss associated with free-carrier absorption. Devices were fabricated from several wafer growths. The composition of the InGaAsP well material was altered between wafer growths to vary the photoluminescence wavelength between 1420 and 1450 nm. Linear absorption measurements did not show sharp excitonic features, revealing well-barrier interface roughness and/or well-to-well thickness variations.

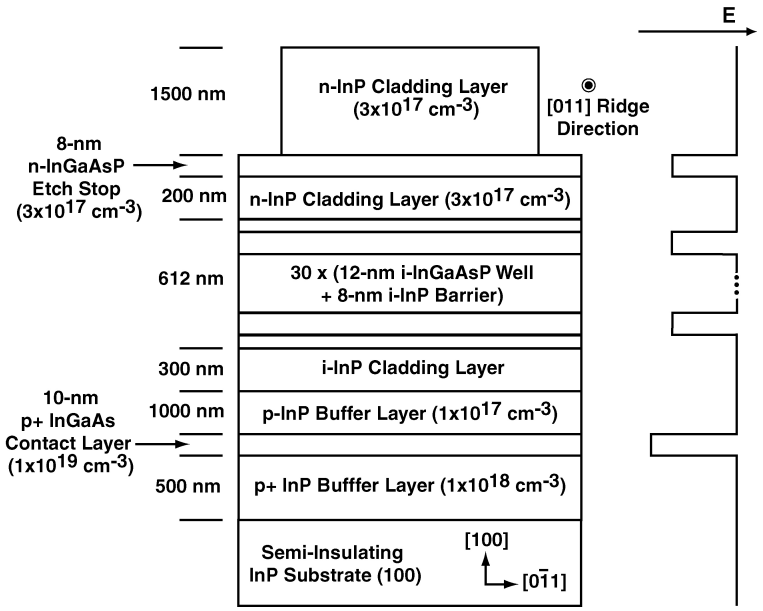


**Fig. 2**. Epitaxial material design of n-i-p InGaAsP/InP symmetric, uncoupled quantum-well electrorefractive modulator.

Figure 3 shows a top-view of the MZ modulator structure with S-bend Y-branch splitter/combiners and push-pull electrodes. The modulator waveguides were defined using three $CH_4$-$H_2$-Ar RIE process steps. First, lateral optical confinement was obtained using a strip-loaded rib etched to the InGaAsP etch-stop layer. Rib widths of w = 2.0, 2.5, 3.0, 3.5, and 4.0 μm were fabricated. Second, the n-i-p electrical width was defined using a 12-μm ridge etched to the InGaAs contact layer. Third, the individual modulators were isolated by etching to the semi-insulating InP substrate. For some of the devices, the first etch-step was designed to go through the n and i layers to the p layer and the second etch-step was omitted. The waveguides were coated with 290-nm of $SiO_2$ to provide electrical isolation. The n-contacts on top of the waveguides were formed using a Ni-Ge-Au liftoff. The p-contacts and interconnect metal were formed by sputter/etching Ti-Au. Both contacts were simultaneously alloyed at 450°C for 30 s. Devices were fabricated with electrode lengths of $L_E$ = 1, 3, and 10 mm. The S-bends used in the Y-branches had a conservative minimum radius of 10 mm. The length added by each Y-branch, including a straight waveguide input/output section, was 3 mm.

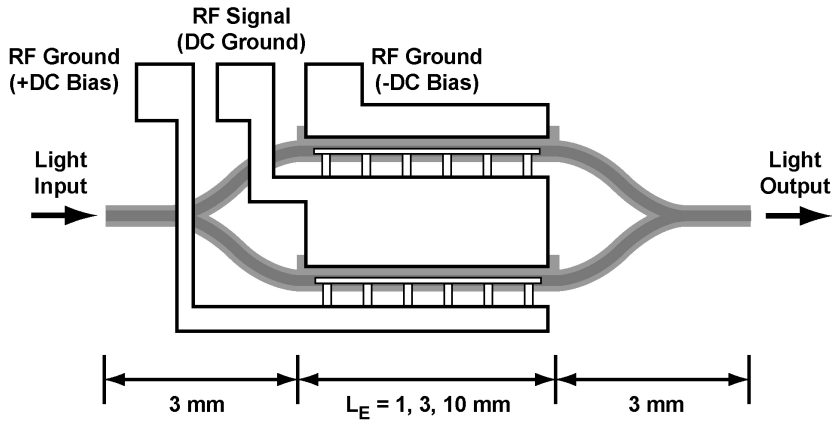


**Fig. 3**. Top-view schematic of electrorefractive Mach-Zehnder modulator with push-pull electrodes.

## 3. MEASUREMENT RESULTS

The DC transmission characteristic (Fig. 4) of a modulator having w = 3 μm, $L_E$ = 10 mm, and a total device length of $L_T$ = 16 mm reveals a push-pull $V_\pi$ = 0.9 V, a fiber-to-fiber insertion loss of 18 dB, and an extinction ratio of 14 dB. The voltage-length ($V_\pi$-L) product for this modulator (9 V-mm) is a factor 5 to 7 smaller than that of typical $LiNbO_3$ modulators.[25] Input and output coupling was achieved using lensed fibers having a 1/e-mode-field diameter of 2.5 μm. The bias voltage across the push-pull diode pair was 5 V. The measurement wavelength (1560 nm) was 140 nm larger than the bandedge wavelength. The combination of the linear and quadratic electro-optic effects provides a nearly sinusoidal intensity response (dotted line) for small push-pull voltage deviations around the equal bias condition. The deviation of the measured response from sinusoidal at large push-pull voltages is attributed to a combination of the nonlinear electro-optic and electroabsorptive effects. The observed extinction ratio of different MZ modulators ranged from 14 to 20 dB. This variation in extinction ratio is attributed to multi-mode operation of the double ridge waveguide. The single-etch ridge modulators exhibited extinction ratios of ~20 dB independent of input fiber alignment.

Fabry-Perot cut-back loss measurements were performed on a straight-waveguide phase modulator (w = 3 μm) fabricated on a wafer different from the modulator described above. The measurements were conducted by sweeping the wavelength of a tunable laser and observing the Fabry-Perot transmission response of the unbiased phase-modulator waveguide. The waveguide was cleaved from a length of 13 mm to 5mm in 2-mm decrements and the normalized contrast-ratio $K = (T_{MAX} - T_{MIN})/(T_{MAX} + T_{MIN})$ was determined for each length. The resulting data are plotted in Fig. 5 using the conventional waveguide-loss analysis.[26] The slope and intercept obtained from a linear fit to the data reveal a material/waveguide loss of 7 dB/cm ($\alpha$ = 1.6 $cm^{-1}$) and a Fresnel facet-reflectivity of 28%, respectively. A fiber-to-waveguide coupling loss of 5 dB/facet was determined by subtracting the material/waveguide loss estimate from the total measured fiber-to-fiber insertion loss. The coupling loss consists of both the Fresnel-reflection loss (1.4 dB/facet) and the mode-mismatch loss. Thus, the mode-mismatch loss is 3.6 dB/facet. This value is larger than the mode-mismatch loss of 1.9 dB/facet predicted via mode-overlap calculations. The insertion loss of MZ modulators fabricated on the same chip as the phase modulators was also measured. The loss of the Y-branch splitter/combiner used in the MZ modulator was calculated to be 0.85 dB by combining the loss data from the MZ and phase modulators.

Figure 6 depicts the wavelength-dependent tradeoff between $V_\pi$ and optical insertion loss for a MZ modulator (3-mm electrode length) that results from operation at wavelengths within ~100 nm of the absorption bandedge wavelength. The peak photoluminescence wavelength for the quantum-well material used to fabricate this modulator

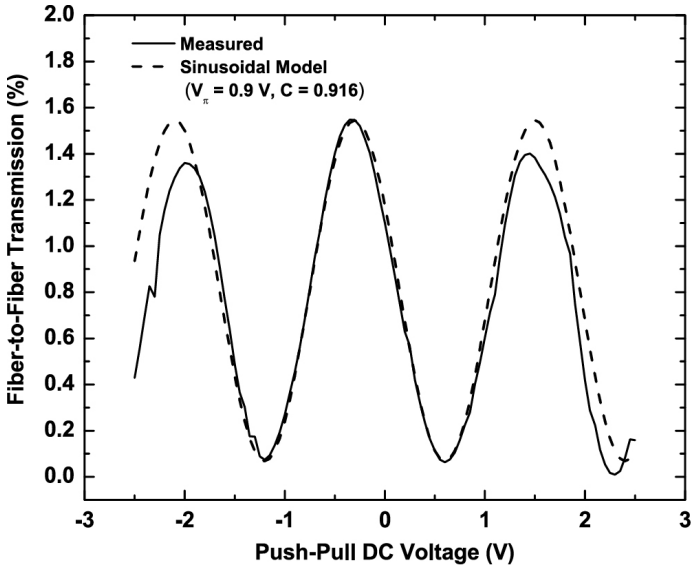


**Fig. 4**. Fiber-to-fiber DC transmission characteristic (solid line) of InGaAsP/InP electrorefractive modulator with 10-mm-long push-pull electrodes. Sinusoidal model (dotted line) also shown. C = contrast ratio. $\lambda$ = 1560 nm.

was 1440 nm. At the largest wavelength measured (1580 nm), $V_\pi$ is relatively large (2.6 V) and the insertion loss is relatively small (17.5 dB). As the optical wavelength decreases and approaches the bandedge wavelength, $V_\pi$ decreases and the optical loss increases. At 1520 nm, $V_\pi$ has decreased by a factor of 2, but the insertion loss has increased by almost 10 dB. Thus, the figure-of-merit $T_{MAX}/V_\pi$ decreases as the operating wavelength approaches the bandedge wavelength.

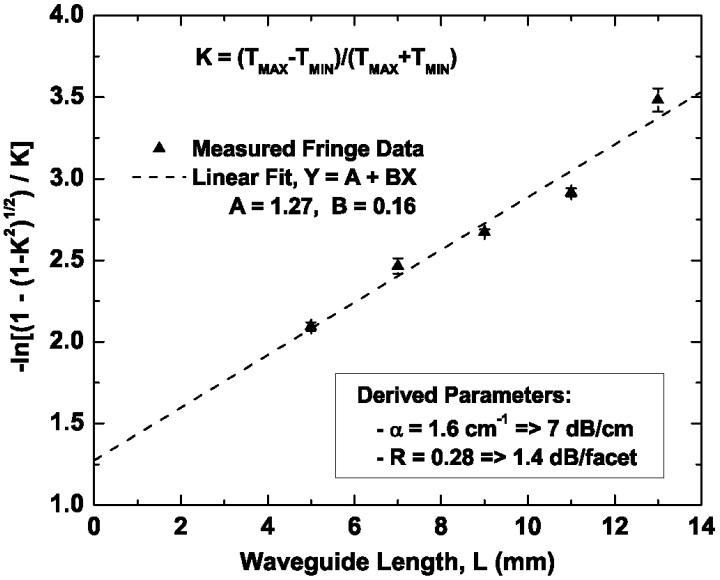


**Fig. 5**. Waveguide loss data obtained from an unbiased phase modulator using the scanned-wavelength Fabry-Perot cutback measurement technique. Waveguide width = 3 µm. Center wavelength = 1570 nm.

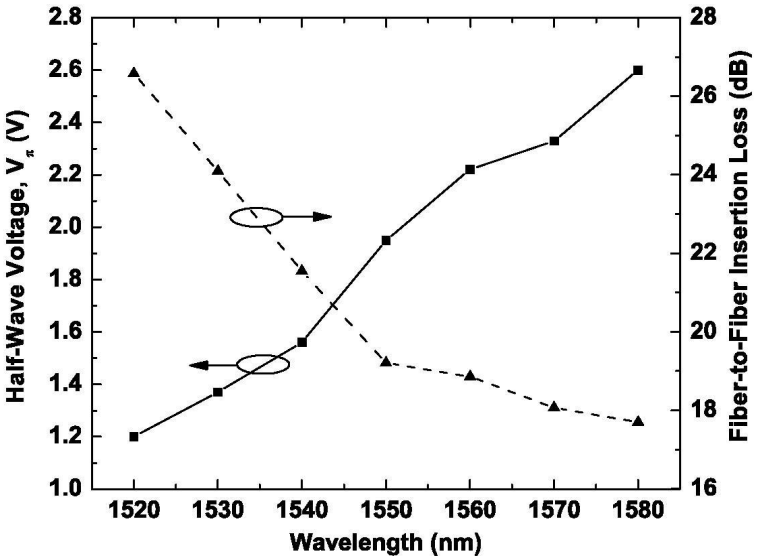


**Fig. 6**. Wavelength dependence of the half-wave voltage $V_\pi$ (squares, solid line) and fiber-to-fiber insertion loss (triangles, dotted line) of a Mach-Zehnder modulator. Lumped-element electrode length = 3 mm. Waveguide width = 3 µm.

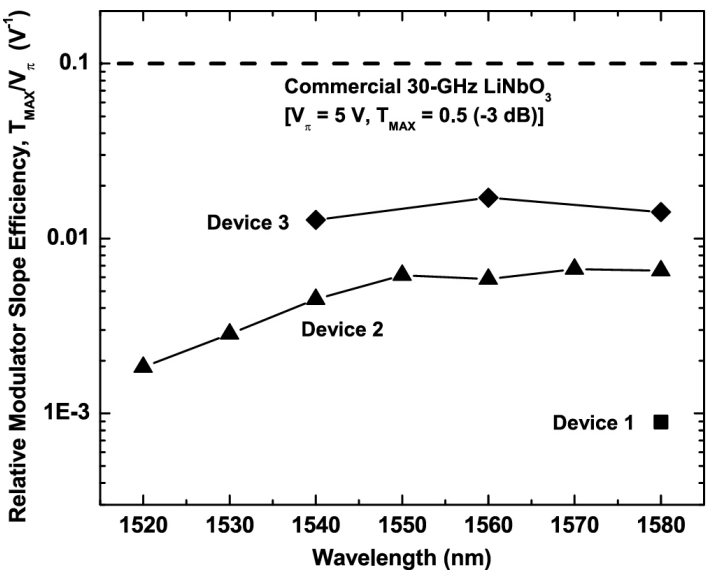


**Fig. 7** Relative modulator slope efficiency $T_{MAX}/V_\pi$ versus wavelength for several generations of push-pull electrorefractive modulators. The efficiency of a commercial 30-GHz $LiNbO_3$ modulator (dotted line) is shown for comparison.

The wavelength dependence of $T_{MAX}/V_\pi$ is more clearly seen in Fig. 7 where the performance of several device generations fabricated from different growths are plotted. The $T_{MAX}/V_\pi$ performance of our modulators has improved with time by more than an order of magnitude due to improvements in material quality and device fabrication. At wavelengths far from the bandedge, $T_{MAX}/V_\pi$ is relatively independent of wavelength. As the bandedge is approached, $T_{MAX}/V_\pi$ decreases (see Device 2 data in Fig. 7). The best value of $T_{MAX}/V_\pi$ that we have obtained is about a factor of 6 smaller than that of commercial wideband $LiNbO_3$ modulators (see dotted line in Fig. 7). This difference in performance can be attributed to the high fiber-to-waveguide coupling loss (5 dB/facet) of the ER modulator. If the coupling loss could be reduced to 1 dB/facet through a combination of anti-reflection coating and mode matching, $T_{MAX}/V_\pi$ of the ER modulators would equal that of current $LiNbO_3$ modulators.

One potential approach for reducing the coupling loss is the use of an inverse laterally tapered optical mode-converter.[27] To investigate the use of this monolithically integrated mode converter with the ER modulators, we performed an eigenmode expansion analysis of the inverse-taper structure. We note that the results of the eigenmode expansion technique agree well with full three-dimensional finite-difference time-domain (FDTD) simulations for similar taper structures. The simulated waveguide thickness was 0.4 μm with an index of $n_{CORE}$ = 3.32 meant to represent the rms index of the multiple quantum-well active region. Note that this thickness is smaller than the 0.61-μm thickness of the active region used in our present structures. The waveguide width was exponentially tapered from 0.4 μm at the fiber-input interface to 1.6 μm representing the final waveguide width. The cladding above and below the taper was InP with an index of $n_{CLAD}$ = 3.17. To realize this mode converter, material regrowth would be required to deposit the InP upper-cladding layer. Figure 8 shows the coupling efficiency between a lensed fiber (1/e-field diameter = 2.5 μm) and the output of the mode converter as a function of exponential-taper length. The coupling-efficiency calculation assumes a perfect anti-reflection coating. The simulation results indicate that a coupling efficiency of 88% (-0.6 dB) can be obtained with a taper length of only a few hundred microns.

The frequency response of a lumped-element ($L_E$ = 1 mm) MZ modulator is shown in Fig. 9. The frequency response characteristic is well fit using a single-pole RLC model (R = 50 Ω, L = 14 nH, C = 3 pF). The 3-dB bandwidth was measured to be 1.2 GHz. The bandwidth of the $L_E$ = 10 mm modulator is expected to be ~120 MHz since the response of the lumped-element electrode is capacitance limited. Traveling-wave electrodes are required to increase the modulator bandwidth.

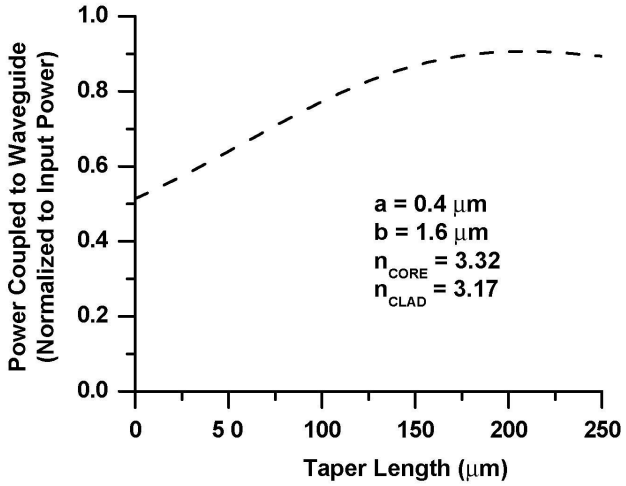


**Fig. 8**. Coupling efficiency between a lensed fiber (1/e-field diameter = 2.5 μm) and the output of an inverse laterally tapered mode-converter as a function of the exponential taper length. Waveguide thickness = 0.4 μm. Input taper width: a = 0.4 μm. Output taper width: b = 1.6 μm.

To investigate the linearity of the electrorefractive modulators, two-tone measurements were performed on a MZ modulator having a 3-mm-long electrode. The measurements were performed by applying a two-frequency, equal-amplitude signal to the modulator, detecting the modulated optical signal using a wideband (7 GHz) InGaAs p-i-n photodiode, and observing the detected fundamental and third-order intermodulation signals on a microwave spectrum analyzer. The two-tone signal was generated by combining, filtering and amplifying the outputs of two RF synthesizers. The input RF frequencies were 178 and 180 MHz. The optical power at the modulator input was 3 mW. The measurements were conducted with the modulator biased at quadrature where the DC output power and detected current were 26 μW and 18 μA, respectively. At this low detected current, the shot-noise level (-185 dBm/Hz) is below the thermal-noise floor (-174 dBm/Hz).

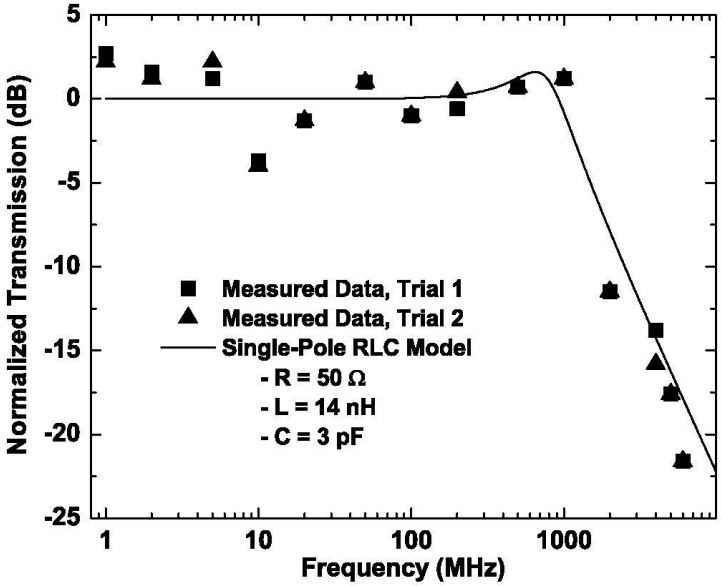


**Fig. 9**. Small-signal frequency response of an electrorefractive Mach-Zehnder modulator with a lumped-element electrode. Single-pole RLC model (solid line) also shown with parameters R = 50 Ω, L = 14 nH, and C = 3 pF. Electrode length = 1 mm. Waveguide width = 3 μm.

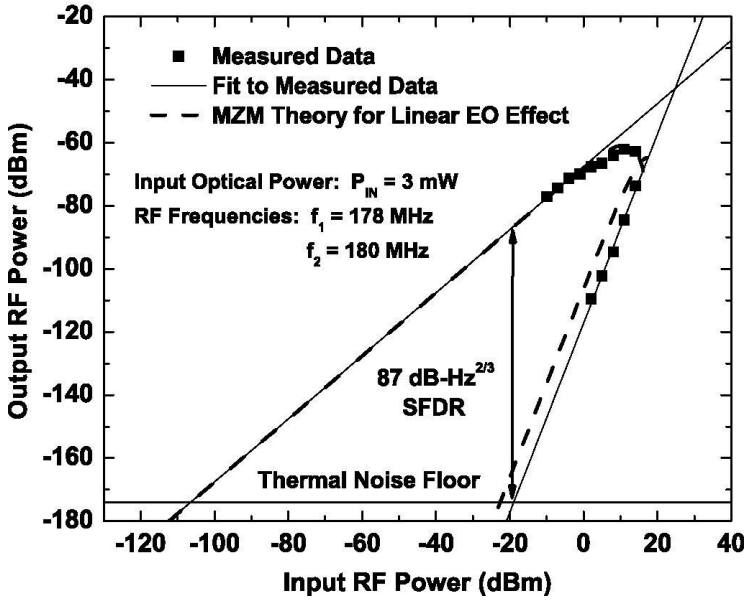


**Fig. 10**. Two-tone intermodulation performance of an electrorefractive Mach-Zehnder modulator showing the detected output power of the fundamental signal and 3rd-order intermodulation spurs as a function of the single-tone input power. Modulator biased at quadrature. Electrode length = 3 mm. Waveguide width = 2 μm (single deep etch).

The results of the two-tone measurements (Fig. 10) reveal a third-order spur-free dynamic range (SFDR) of 87 dB-$Hz^{2/3}$. This relatively low SFDR results primarily from the high insertion loss (17.6 dB) of the modulator. Reducing the total coupling loss from 10 to 2 dB would increase the SFDR by about 11 dB. However, some optical saturation of the modulator response was observed at the 3-mW input optical power. This saturation may limit the improvement that could be obtained by reducing the coupling loss. Also shown in Fig. 10 are the theoretical responses of the fundamental signal and third-order intermodulation spurs for a MZ modulator incorporating a material that has a linear phase-vs-voltage electro-optic effect.[28] The parameters of the theoretical model were adjusted to optimize the fit to the fundamental signal data, including compression at high RF input power. The third-order intermodulation spur power versus input RF power was then calculated using the same parameters. The calculated third-order curve lies to the left of the measured data indicating that the linearity of the ER modulator is better than that of a MZ modulator using the linear electro-optic effect. The SFDR relative improvement for the ER modulator is about 3 dB.

## 4. CONCLUSIONS

We have shown that the modulator slope efficiency of ER modulators incorporating symmetric, uncoupled quantum wells could be made to equal that of $LiNbO_3$ modulators given improved optical coupling efficiency. We note that linear absorption measurements have revealed significant inhomogeneous broadening of the absorption bandedge of our quantum-well material. This broadening is expected to reduce $T_{MAX}/V_\pi$ by both increasing the below-bandedge absorption and reducing the electrorefractive strength. Thus, improvements in material quality are expected to improve the $T_{MAX}/V_\pi$ of symmetric, uncoupled quantum wells beyond what has been reported here. Additionally, the use of stepped quantum-wells[23] or asymmetric coupled quantum-wells[22] should allow the ER slope efficiency to be significantly greater than that of $LiNbO_3$ devices. The asymmetric coupled quantum-wells are especially attractive since the electrorefractive effect in these structures is not accompanied by a large bandedge shift that modulates the below-bandedge absorption. The higher electrorefractive efficiency of the advanced quantum-well materials would also reduce the required electrode length relative to standard quantum wells. This reduced electrode-length would relax the velocity-matching requirement for wideband traveling-wave electrodes.

## ACKNOWLEDGEMENTS

This work was sponsored by the DARPA Radio-Frequency Lightwave Integrated Circuits (RFLICS) program under Air Force Contract No. F19628-00-C-0002. The opinions, interpretations, conclusions, and recommendations are those of the authors and are not necessarily endorsed by the United States Government.

## REFERENCES

1. J. E. Roman, L. T. Nichols, K. J. Williams, R. D. Esman, G. C. Tavik, M. Livingston, and M. G. Parent, "Photonic remoting of the receiver of an ultra-high dynamic range radar," in *Proc. IEEE MTT-S International Microwave Symposium*, 1998, pp. 1521-1524.
2. W. Ng, A. A. Walston, G. L. Tangonan, J. J. Lee, I. L. Newberg, and N. Bernstein, "The first demonstration of an optically steered microwave phased array antenna using true-time-delay," *J. Lightwave Technol.*, vol. 9, pp. 1124-1131, 1991.
3. A. Hirata, M. Harada, K. Sato, and T. Nagatsuma, "Low-cost millimeter-wave photonic techniques for gigabit/s wireless link," *IEICE Trans. Electron.*, vol. E86-C, pp. 1123-1128, 2003.
4. C. I. Cox, E. Ackerman, R. J. Helkey, and G. E. Betts, "Techniques and performance of intensity-modulation direct-detection analog optical links," *IEEE Trans. Microwave Theory Tech.*, vol. 45, pp. 1375-1383, 1997.
5. C. I. Cox and W. S. C. Chang, "Figures of merit and performance analysis of photonic microwave links," in *RF Photonic Technology in Optical Fiber Links*, W. S. C. Chang, Ed. Cambridge: Cambridge University Press, 2002, pp. 1-33.
6. "EOSPACE 40-Gb/s Modulator Specification Sheet," EOSPACE, Inc. 2003.
7. K. K. Loi, J. H. Hodiak, X. B. Mei, C. W. Tu, W. S. C. Chang, D. T. Nichols, L. J. Lembo, and J. C. Brock, "Low-loss 1.3-μm MQW electroabsorption modulators for high-linearity analog optical links," *IEEE Photon. Technol. Lett.*, vol. 10, pp. 1572-1574, 1998.
8. J. Cole, Naval Research Laboratory, Private communication, 2004.
9. K. Djordjev, S.-J. Choi, S.-J. Choi, and P. D. Dapkus, "Vertically coupled InP microdisk switching devices with electroabsorptive active regions," *IEEE Photon. Technol. Lett.*, vol. 14, pp. 1115-1117, 2002.
10. B. Liu, J. Shim, Y.-J. Chiu, H. F. Chou, J. Piprek, and J. E. Bowers, "Slope efficiency and dynamic range of traveling-wave multiple-quantum-well electroabsorption modulators," *IEEE Photon. Technol. Lett.*, vol. 16, pp. 590-592, 2004.
11. J. X. Chen, Y. Wu, W. X. Chen, I. Shubin, A. Clawson, W. S. C. Chang, and P. K. L. Yu, "High-power intrastep quantum well electroabsorption modulator using single-sided large optical cavity waveguide," *IEEE Photon. Technol. Lett.*, vol. 16, pp. 440-442, 2004.
12. J. S. Cites and P. R. Ashley, "High-performance Mach-Zehnder modulators in multiple quantum well GaAs/AlGaAs," *J. Lightwave Technol.*, vol. 12, pp. 1167-1173, 1992.
13. C. Rolland, R. S. Moore, F. Shepard, and G. Hillier, "10Gbit/s, 1.56μm multiquantum well InP/InGaAs Mach-Zehnder optical modulator," *Electron. Lett.*, vol. 29, pp. 471-472, 1993.
14. M. Fetterman, C.-P. Chao, and S. R. Forrest, "Fabrication and analysis of high-contrast InGaAsP-InP Mach-Zehnder modulators for use at 1.55-μm wavelength," *IEEE Photon. Technol. Lett.*, vol. 8, pp. 69-71, 1996.
15. P. W. Juodawlkis, F. J. O'Donnell, R. J. Bailey, J. J. Plant, K. G. Ray, D. C. Oakley, A. Napoleone, and G. E. Betts, "Sub-volt-$V_\pi$ InGaAsP electrorefractive modulators using symmetric, uncoupled quantum wells," in *Proc. IEEE LEOS Annual Meeting*, 2003, pp. 788-789.
16. I. Bar-Joseph, C. Klingshirn, D. A. B. Miller, D. S. Chemla, U. Koren, and B. I. Miller, "Quantum-confined Stark effect in InGaAs/InP quantum wells grown by organometallic vapor phase epitaxy," *Appl. Phys. Lett.*, vol. 50, pp. 1010-1012, 1987.
17. D. A. B. Miller, J. S. Weiner, and D. S. Chemla, "Electric-field dependence of linear optical properties in quantum well structures: waveguide electroabsorption and sum rules," *IEEE J. Quantum Electron.*, vol. 22, pp. 1816-1830, 1986.
18. G. L. Li and P. K. L. Yu, "Optical intensity modulators for digital and analog applications," *J. Lightwave Technol.*, vol. 21, pp. 2010-2030, 2003.

19. R. B. Westland, J. T. Zhu, W. X. Chen, A. R. Clawson, P. K. L. Yu, and S. A. Pappert, "Combined Franz-Keldysh and quantum-confined Stark effect waveguide modulator for analog signal transmission," *J. Lightwave Technol.*, vol. 17, pp. 497-502, 1999.
20. J. E. Zucker, I. Bar-Joseph, B. I. Miller, U. Koren, and D. S. Chemla, "Quaternary quantum wells for electro-optic intensity and phase modulation at 1.3 and 1.55 µm," *Appl. Phys. Lett.*, vol. 54, pp. 10-12, 1989.
21. J. S. Weiner, D. A. B. Miller, and D. S. Chemla, "Quadratic electro-optic effect due to the quantum-confined Stark effect in quantum wells," *Appl. Phys. Lett.*, vol. 50, pp. 842-844, 1987.
22. C. Thirstrup, "Refractive index modulation based on excitonic effects in GaInAs-InP coupled asymmetric quantum wells," *IEEE J. Quantum Electron.*, vol. 31, pp. 988-996, 1995.
23. H. Mohseni, Z. Shellenbarger, M. H. Kwakernaak, A. Lepore, and J. H. Abeles, "Highly sensitive InP-based phase modulators based on stepped quantum wells," in *Proc. Conference on Lasers and Electro-Optics*, 2003, pp. CTuJ4.
24. H. Feng, J. P. Pang, M. Sugiyama, K. Tada, and Y. Nakano, "Field-induced optical effect in five-step asymmetric coupled quantum well with modified potential," *IEEE J. Quantum Electron.*, vol. 34, pp. 1197-1208, 1998.
25. G. E. Betts, "$LiNbO_3$ external modulators and their use in high performance analog links," in *RF Photonic Technology in Optical Fiber Links*, W. S. C. Chang, Ed. Cambridge: Cambridge University Press, 2002, pp. 81-132.
26. E. Kapon and R. Bhat, "Low-loss single-mode GaAs/AlGaAs optical waveguides grown by organometallic vapor phase epitaxy," *Appl. Phys. Lett.*, vol. 50, pp. 1628-1630, 1987.
27. K. Kasaya, O. Mitomi, M. Naganuma, Y. Kondo, and Y. Noguchi, "A simple laterally tapered waveguide for low-loss coupling to single-mode fibers," *IEEE Photon. Technol. Lett.*, vol. 5, pp. 345-347, 1993.
28. B. H. Kolner and D. W. Dolfi, "Intermodulation distortion and compression in an integrated electrooptic modulator," *Appl. Opt.*, vol. 26, pp. 3676-3680, 1987.